Journal of Thermal Analysis and Calorimetry
https://doi.org/10.1007/s10973-020-10035-z

Experimental energy and exergy performance of an automotive heat pump using R1234yf

Alpaslan Alkan[1] · **Ahmet Kolip**[1] · **Murat Hosoz**[2]

Received: 18 February 2020 / Accepted: 3 July 2020

Abstract

Various energy and exergy performance parameters of an automotive heat pump (AHP) with R1234yf have been investigated and compared with those of the baseline system with R134a. For this aim, an AHP system was set up from the components of an air-conditioning system employed in a compact car and equipped with instruments for mechanical measurements. It was tested with R1234yf and R134a by changing the compressor speed and air stream temperatures incoming the outdoor and indoor units. Using test data, energy and exergy analyses of the AHP were performed, and its performance parameters were evaluated. The R1234yf system provided conditioned air temperatures in the range of 29.9–59.3 °C, heating capacities in the range of 1.96–3.14 kW and coefficient of performance (COP) values in the range of 2.44–4.56. It yielded 3.3–10.8 °C lower conditioned air temperature, 9.2–15.4% lower heating capacity, 1.6–7.1% lower COP, 13.8–21.6 °C lower compressor discharge temperature, 3.1–19.2% higher total exergy destruction rate per unit heating capacity but significantly less TEWI in comparison with the system with R134a. Moreover, the R1234yf system yielded larger exergy destructions in the outdoor unit, compressor and expansion device but lower exergy destruction in the indoor unit. These findings reveal that R1234yf can be used in AHP systems in expense of less heating capacity, lower COP and higher exergy destruction rate per unit heating capacity in comparison with R134a.

Keywords Heat pump · Automotive · R1234yf · R134a · Exergy

Abbreviations

AAC	Automotive air-conditioning
AHP	Automobile heat pump
COP	Coefficient of performance
D_{ann}	Annual driving distance/km
EU	European Union
EV	Electric vehicle
FC_m	Volumetric fuel consumption per 100 kg mass of the AHP in 10,000 km driving/L
FC_{pow}	Volumetric fuel consumption in 10,000 km to power the AHP using R134a/L
GWP	Global warming potential
HFC	Hydrofluorocarbon
HFO	Hydrofluoroolefin
ODP	Ozone depleting potential
PTC	Positive temperature coefficient
TEWI	Total equivalent warming impact
TFA	Trifluoroacetic acid
TXV	Thermostatic expansion valve
V	Hand valve

List of symbols

c_p	Specific heat/kJ kg^{-1} K^{-1}
$\dot{E}x_d$	Rate of exergy destruction/kW
h	Specific enthalpy/kJ kg^{-1}
L	Annual refrigerant leakage ratio
m_{AHP}	Mass of the AHP system/kg
m_r	Refrigerant charge/kg
$\dot{m}$	Mass flow rate/kg s^{-1}
N	Lifetime of the system/year
n	Number of measured variables
P	Pressure/kPa
$\dot{Q}$	Heat transfer rate/kW
R	Ideal gas constant/kJ kg^{-1} K^{-1}

✉ Murat Hosoz
mhosoz@kocaeli.edu.tr

Alpaslan Alkan
aalkan@subu.edu.tr

Ahmet Kolip
akolip@subu.edu.tr

[1] Department of Mechanical Engineering, Sakarya University of Applied Sciences, 54187 Sakarya, Turkey

[2] Department of Automotive Engineering, Kocaeli University, 41001 Kocaeli, Turkey

Published online: 13 July 2020

s	Specific entropy/kJ kg^{-1} K^{-1}
T	Temperature/K or °C
u	Uncertainty
$\dot{W}$	Power/kW
x	Measured variable
y	Function of measured variables

Greeks

α	Refrigerant recovery factor
β	CO_2 emission factor of the fuel/kg CO_2 L^{-1}
ω	Specific humidity
ψ	Specific flow exergy/kJ kg^{-1}

Subscripts

0	Dead state
a	Air
ai	Air inlet
comp	Compressor
cv	Control volume
in	Inlet
iu	Indoor unit
j	Location on the boundary
ou	Outdoor unit
out	Outlet
r	Refrigerant
tot	Total
v	Water vapour

Introduction

Fast industrialization in the past decades has led to some environmental problems such as depletion of the ozone layer and global warming. Automotive air-conditioning (AAC) systems have been one of the sources of these problems. AAC systems initially employed R12, a refrigerant from chlorofluorocarbon family. Noticing that refrigerants containing chlorine were harmful for the ozone layer, their use was restricted by the Montreal Protocol in 1987 [1], and it was decided to change to more environmentally friendly fluids. Then, automotive manufacturers started to use R134a, a refrigerant from hydrofluorocarbon (HFC) family, with no ozone depleting potential (ODP). However, R134a was subjected to a phase-down by the Kyoto Protocol in 1997 due to its high global warming potential (GWP), namely 1430 [2]. Then, European Union (EU) issued an F-gas regulation [3] banning the use of refrigerants with a GWP exceeding 150 in the AAC systems of vehicles put on the EU market starting from 2017. The Kyoto Protocol and F-gas regulation have accelerated the investigations on alternative refrigerants. Potential alternatives to replace R134a have been determined as CO_2 (R744), R152a and two recently developed refrigerants from hydrofluoroolefin (HFO) family, namely R1234yf and R1234ze(E) [4]. Operating pressures of supercritical R744 systems are about 7–10 times higher than those of conventional R134a systems [5]. Therefore, the components of the AAC systems using R744 should withstand compressor discharge pressures of as high as 150 bars without leakage, which leads to heavy equipment and poor heat transfer due to increased wall thickness. On the other hand, high flammability of R152a restricts its use in AAC systems. Although it is also slightly flammable and much more expensive than R134a, with a GWP of less than 1 [6], zero ODP and higher energy effectiveness than R1234ze(E), R1234yf is considered as the best alternative to R134a [7]. It can also be used as a retrofit refrigerant in existing AAC systems with R134a.

The vehicles with internal combustion engines usually have plenty of waste heat rejected into the engine coolant. However, electric vehicles (EVs) lack waste heat to be used for the comfort heating of the passenger cabin. Therefore, innovative air-conditioning systems with heat pump function, which are appropriate for both cooling and heating the passenger compartment of EVs, have been recently studied as reviewed by Peng and Du [8]. Automotive heat pump (AHP) systems can also be used for providing supplementary heating if the vehicle is equipped with a high efficiency internal combustion engine, thus having insufficient waste heat for comfort heating.

Tamura et al. [9] evaluated the experimental performance of an AHP with R744, finding that it had equal or slightly better performance than the AHP with R134a. Wang et al. [10] also investigated the performance of an AHP using R744 and obtained the coefficient of performance (COP) for the system as 1.7 at −20 °C ambient temperature. Moreover, Wang et al. [11] determined that the AHP system with R744 could operate more efficiently than the conventional positive temperature coefficient (PTC) heaters.

Hosoz and Direk [12] investigated the experimental performance of an R134a AHP in both heating and cooling operations, obtaining that the heating operation provided enough heating only in mild weather conditions, while it yielded a higher COP than the cooling operation. Lee et al. [13] evaluated various performance parameters of an R134a AHP for an electric bus utilizing the heat wasted by electric devices as the heat source. They determined that the heating capacity increased but COP decreased with rising outdoor air temperature and compressor speed. Hosoz et al. [14] developed an R134a AHP operated by a diesel engine and evaluated the steady-state and transient performance merits of the AHP for various heat sources, namely outdoor air, engine coolant and exhaust gas. They found that the AHP with engine coolant provided the largest heating capacity and COP, whereas the one using ambient air provided the lowest ones. Wang et al. [15] developed an AHP for EVs and evaluated its performance for R134a and R407C. They determined that the heating capacity of the R407C system was higher, but its COP was lower compared to the R134a

system. Lee and Lee [16] studied the performance of an AHP using R134a for EVs. They reported the heating capacity and COP as 3.10 kW and 3.26, respectively, for − 10 °C outdoor temperature. Their results showed that the heating capacity was insufficient to provide thermal comfort in the passenger cabins of EVs.

After the development of refrigerants from HFO family meeting the F-gas regulation, investigations have been concentrated on their use as alternatives to R134a in AAC systems. Zilio et al. [17] studied on the effects of using R1234yf instead of R134a in an experimental AAC system, finding that R1234yf provided a lower cooling capacity and COP. Mota-Babiloni et al. [18] investigated the experimental performance of R1234yf, R1234ze(E) and R134a in a vapour compression refrigeration system using an open-type compressor, shell and tube evaporator and shell and tube condenser. They reported that the R1234yf system yielded on average 9% lower cooling capacity and 7% less COP compared to the R134a system. Cho and Park [19] evaluated the performance parameters of an R1234yf AAC system by applying energy and exergy analyses to it. They reported that the R1234yf system yielded 4.0–7.0% lower cooling capacity, 3.6–4.5% less COP and 0.5–3.3% higher total exergy destruction rate compared with the R134a system. Prabakaran et al. [20] added an internal heat exchanger to an R134a AAC system and operated it with refrigerants R134a and R1234yf. They observed that the tuning of the thermostatic expansion valve in the R1234yf system had a positive influence on the COP, cooling capacity and exergy efficiency in the ranges of 4.3–8.6%, 6.5–10.1% and 3.7–5.1%, respectively, relative to the R134a system at idling and city speed conditions. With the aim of increasing the COP and volumetric capacity of R1234yf while reducing GWP of HFCs, Huang [21] compared the performance of HFC/R1234yf mixtures using verified thermodynamic models. He found that R134a/R1234yf mixtures required little change in the compressor size, and considering both GWP and efficiency, the optimal composition for R134a/R1234yf was 10/90%.

Some investigations focussed on R134a alternatives with higher thermodynamic performance in comparison with R1234yf. Abraham and Mohanraj [22] evaluated experimental performance of an AAC system using R430a as a drop-in substitute of R134a. They found that the COP of the AAC system with R430a was 12–20% higher, while its exergy destruction rate was 12–28% lower in comparison with the system with R134a. Gill et al. [23] determined the irreversibility in the components of a vapour compression refrigeration system using R134a/LPG mixture as a replacement for R134a. They reported that the irreversibilities in the components of the system using R134a/LPG mixture were lower relative to the R134a system. Then, they developed artificial neural network models to predict the second law efficiency and total irreversibility of the system. Gill et al. [24] also evaluated the exergy performance of a vapour compression refrigeration system with R450a as a replacement for R134a. They found that the total irreversibility of the system with R450a was 15.25–27.32% lower and its exergy efficiency was 10.07–130.93% higher relative to the R134a system. They reported that the evaporator was the most efficient component, while the compressor was the least efficient one for both refrigerants.

In addition to AAC investigations, some studies focussed on the performance of AHP systems using R1234yf. Zou et al. [25] developed an R1234yf AHP employing an electric expander valve and a secondary fluid circuit for supplemental heating of EVs. They found that the expander valve opening and working conditions had significant influence on the performance of the system. Direk and Yuksel [26] developed an experimental AHP system and tested its various energy performance parameters for refrigerants R134a, R1234ze(E), R152a and R444a. They reported that R152a yielded the highest heating capacity, while R1234ze(E) resulted in the lowest capacity but the highest COP. Wang et al. [27] developed an integrated AAC and AHP system for an electric vehicle and tested it for refrigerants R134a and R407C. They reported that the system provided a significant heating capacity and reduced the energy consumption required for the comfort heating of the passenger cabin compared to the PTC heater. Zhang et al. [28] performed the exergy analysis of an EV AAC/AHP system integrated with the battery thermal management system of the EV. They determined that the compressor was the main source of the exergy loss in the system for both operation modes and the system exergy loss linearly increased as a function of the compressor speed. They also reported that the heating performance of the system was better than that of the PTC heater. Ozcan et al. [29] performed the exergy analysis of a bus air-conditioning and heat pump system, revealing that its total exergetic efficiencies were 3.41% and 11.92% in cooling and heating modes, respectively. Direk and Yuksel [30] studied various performance parameters of an AAC/AHP system using R134a and R1234yf from the perspective of the first law of thermodynamics. Although their tests yielded lower cooling and heating capacities and COPs for R1234yf in comparison with R134a, they concluded that R1234yf can be used in both cooling and heating applications.

It is seen that numerous investigations have been made to compare the performance of AAC systems using R1234yf and R134a. However, the number of investigations on the performance comparison of AHP systems with these two refrigerants is very limited. In those studies, the tests were usually performed in a narrow range by considering the energy performance of the system. In this study, based on tests conducted in a broad range of operating conditions, various energy and exergy performance merits of an AHP

system with R1234yf were experimentally evaluated and compared with those of the system with R134a.

Experimental system and test procedure

The schematic layout of the experimental AHP is indicated in Fig. 1. It was developed by adding some extra components to the refrigeration circuit of the air-conditioning system employed in a compact automobile. It employs a fixed-capacity seven-cylinder wobble plate compressor, parallel flow micro-channel outdoor unit, laminated indoor unit, liquid receiver, filter/drier, reversing valve, two thermostatic expansion valves (TXVs) and five hand valves which are indicated by the symbol V in Fig. 1. The technical specifications of these components are reported in Table 1.

The compressor was operated by a 5.5-kW three-phase asynchronous electric motor via a frequency inverter to run it at desired speeds. The indoor unit, which was originally an evaporator, and the outdoor unit, which was originally a condenser, were located into separate 100-cm-long air ducts. The indoor and outdoor air ducts have their own electric heaters with the heating capacities of 1.8 and 5.4 kW, respectively. They were located upstream of the units to obtain the desired air temperatures at their inlets. A twin axial fan arrangement provided an outdoor air stream with an average speed of 3.6 m s^{-1} while a

Table 1 Technical specifications of the components of the experimental AHP

Component	Specification
Compressor	Type: seven-cylinder wobble plate fixed capacity Stroke volume: 154.90 cm^3 r^{-1}
Outdoor unit	Type: parallel flow micro-channel Dimensions: 630 mm × 380 mm × 20 mm Number of channels: 37
Indoor unit	Type: laminated Dimensions: 235 mm × 220 mm × 65 mm Number of channels: 20
Expansion valves	Type: internally balanced thermostatic expansion valves Capacity: 5.5 kW

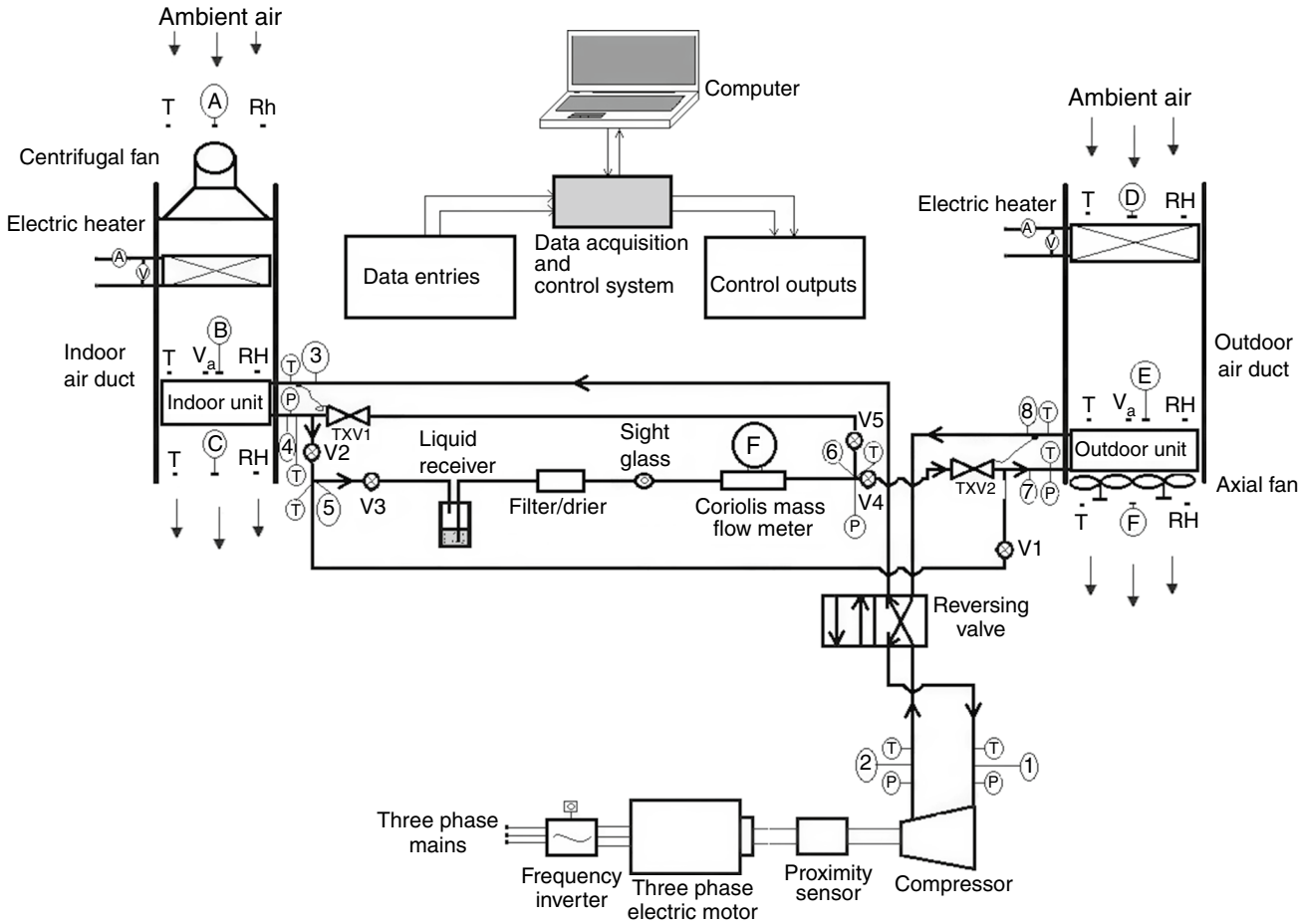

Fig. 1 Schematic layout of the experimental AHP

centrifugal fan provided an indoor air stream with an average speed of 1.5 m s^{-1}.

Figure 1 also indicates the points at which mechanical measurements such as pressure, temperature, relative humidity, refrigerant flow rate, air speed and compressor speed were performed. The refrigerant mass flow rate was measured by a Coriolis mass flow meter placed downstream of the condenser. The suction and discharge pressures were measured by both pressure transmitters and Bourdon manometers, while the indoor unit outlet pressure, outdoor unit inlet pressure and liquid line pressure were measured by only pressure transmitters. The pressure measurement locations are indicated by the symbol P in Fig. 1. The refrigerant temperatures were measured by T-type thermocouples located at the points indicated by the symbol T. Moreover, the air dry-bulb temperatures and relative humidities were monitored by SHT 71 type temperature/humidity sensors located at the points indicated by the symbols T and RH, respectively. The average air speeds in the ducts were measured by air flow transmitters placed in the positions shown by the symbol V_a. Because a torque sensor was not employed in the system to measure the shaft torque applied to the compressor pulley, the compressor power was determined from the refrigerant side by applying the conservation of energy principle to the compressor as defined in the next section. The compressor speed was measured by an inductive proximity sensor. The data obtained from the sensors were collected by data acquisition cards and transmitted to a computer via a RS485 MODBUS communication protocol. The desired operating conditions were specified by the user in the computer environment, and the operation of the experimental system at these conditions was performed by a PLC, which could change the compressor speed and air temperatures incoming the indoor and outdoor units by controlling the inverter of the compressor electric motor and duct electric heaters, respectively. The specifications of the instruments are reported in Table 2, and a photograph of the AHP system is indicated in Fig. 2.

The refrigerants tested in the experimental AHP system were R134a and R1234yf. Various thermodynamic, transport, environmental and safety properties of these refrigerants are reported in Table 3. Both refrigerants are non-toxic and pure substances with zero ODP. However, having a 100-year GWP of 1430 [2], R134a cannot meet the F-gas regulation of the EU. Although the 100-year GWP of R1234yf was initially calculated as 4 [2], further investigations revealed that its GWP was less than 1 [6]. R134a and R1234yf are classified as non-flammable (A1) and mildly flammable (A2L) refrigerants, respectively, by ASHRAE [21, 31]. R1234yf is an unsaturated organic compound composed of

Table 2 Specifications of the instrumentation

Physical quantity	Instrument	Range	Uncertainty
Refrigerant temperature	Type T thermocouple	−40–350 °C	±0.5 °C
Air dry-bulb temperature	SHT 71 temperature sensor	−40–123 °C	±0.4 °C
Pressure	Vika S–10 transmitter	0–25 bar	±0.25 bar
Relative humidity	SHT 71 humidity sensor	0–100%	±3%
Air velocity	EE65–VCK200 transmitter	0.2–10 m s^{-1}	±0.2 m s^{-1}
Mass flow rate	Krohne Optimass 3300C H04 Coriolis flow meter	0–450 kg h^{-1}	±0.1%

Fig. 2 Photograph of the experimental AHP

Table 3 Thermodynamic, transport, environmental and safety properties of the tested refrigerants [6, 18, 21, 31, 33]

Refrigerant	R134a	R1234yf
Chemical formula	CH_2FCF_3	$C_3H_2F_4$
Molar mass/g mol^{-1}	102.03	114.04
Boiling point/°C	−26.3	−30
Critical point/°C	101.1	94.7
Critical pressure/kPa	4059.3	3382.2
Liquid density @ 0 °C/kg m^{-3}	1294.8	1176.3
Vapour density @ 0 °C/kg m^{-3}	14.428	17.647
Latent heat of vaporization @ 0 °C/kJ kg^{-1}	198.60	163.29
Latent heat of vaporization @ 45 °C/kJ kg^{-1}	157.58	127.36
Liquid viscosity @ 0 °C/μPa s	266.53	208.33
Vapour viscosity @ 0 °C/μPa s	10.726	10.068
Liquid thermal conductivity @ 0 °C/W $m^{-1}K^{-1}$	0.0920	0.0715
Vapour thermal conductivity @ 0 °C/W $m^{-1}K^{-1}$	0.0115	0.0116
ODP	0	0
GWP	1430	< 1
ASHRAE Safety Group	A1	A2L

hydrogen, fluorine and carbon. Its atmospheric oxidation gives trifluoroacetic acid (TFA). Although TFA is corrosive, it is not considered hazardous because its carbon–fluorine bond is stable [32]. R1234yf has an atmospheric life cycle of as short as 11 days, i.e. it degrades very quickly. TFA is biodegradable, and there is no significant risk from TFA formed by the degradation of R134a [32]. All thermodynamic and transport properties of the refrigerants presented in Table 3 were taken from REFPROP 9.1 software [33]. The liquid density of R1234yf is lower and vapour density of R1234yf is higher than the corresponding densities of R134a. The latent heat of vaporization of R1234yf is lower than that of R134a for common evaporating and condensing pressures experienced in AAC systems. The liquid and vapour viscosities of R1234yf are lower relative to the related viscosities of R134a. Furthermore, the liquid thermal conductivity of R1234yf is lower than that of R134a, while the vapour thermal conductivities of both refrigerants are close to each other.

The system was initially tested with an R134a charge of 1850 g, which yielded the best system performance. Then, the R134a was recovered, and in accordance with Cho et al. [34], the system was charged with 1650 g of R1234yf, about 10% less than the R134a charge. The difference between R1234yf and R134a charges was due to about 10% lower liquid density of R1234yf compared with that of R134a.

In AAC systems driven by internal combustion engines, the compressor speed changes as a function of the engine speed and it is about the same as the engine speed. While the idle speed of engines for regular automobiles is typically between 600 and 1000 rpm, the driving speed ranges between 2000 and 3000 rpm. In the tests, the minimum compressor test speed corresponding to engine idle speed was chosen as 800 rpm and the maximum speed was chosen as 2800 rpm. Once the required test speed was specified by the user via the computer connected to the PLC, the compressor speed was immediately adjusted to the required value by the PLC through changing the output voltage frequency of the inverter energizing the electric motor of the compressor.

The system was tested by keeping the air temperatures incoming the indoor and outdoor units simultaneously at the same values, namely 2 °C and 10 °C. For 2 °C incoming air temperature, the compressor speed was varied between 800 and 1600 r min^{-1} with 200 r min^{-1} interval. The compressor speeds exceeding 1600 r min^{-1} for this air inlet temperature yielded sub-zero evaporating temperatures and eventually caused frost formation on the outdoor unit. Therefore, the tests at 2 °C air inlet temperature were not performed at the speeds exceeding 1600 r min^{-1}. Furthermore, the air relative humidity entering the outdoor unit was maintained at 77 ± 8% for both refrigerants in these tests. On the other hand, frost formation on the outdoor unit was not observed in the tests conducted at 10 °C air inlet temperature as a result of rising evaporating temperature. Consequently, these tests were performed in the range of 800–2800 r min^{-1}. Moreover, the relative humidity of the air stream incoming the outdoor unit was maintained at 52 ± 4% for both refrigerants in these tests. Not only the steady-state but also the transient performance of the experimental system was evaluated. The former was achieved using only the steady-state data, which were collected in the last 5 min of the tests.

Energy and exergy analyses of the experimental AHP

The conservation of energy principle was applied to the components of the experimental AHP to evaluate its energy performance parameters by ignoring the pressure drops in the indoor and outdoor units as well as refrigerant lines and assuming that the kinetic and potential energies do not change in the components.

Referring to Fig. 1 and using the conservation of energy principle, the heat transfer rate in the indoor unit, i.e. the heating capacity of the system, can be determined from

$$\dot{Q}_{iu} = \dot{m}_r(h_3 - h_4) \quad (1)$$

where $\dot{m}_r$ is the refrigerant mass flow rate and h is the enthalpy of the refrigerant, which can be obtained from REFPROP 9.1 software [33] as functions of pressure and temperature measurements.

The compressor power transferred to the refrigerant in the adiabatic compressor can be evaluated from

$$\dot{W}_{comp} = \dot{m}_r(h_2 - h_1) \tag{2}$$

The ratio between the heating capacity and compressor power yields the COP for heating, an indicator of the energy effectiveness of the AHP, i.e.

$$\mathrm{COP} = \frac{\dot{Q}_{iu}}{\dot{W}_{comp}} \tag{3}$$

If the exergy rate balance equation is applied to the system components, their thermodynamic inefficiencies can be determined. This equation for control volumes can be written as

$$\sum\left(1 - \frac{T_0}{T_j}\right)\dot{Q}_j - \dot{W}_{cv} + \sum \dot{m}_{in}\psi_{in} - \sum \dot{m}_{out}\psi_{out} = \dot{E}x_d \tag{4}$$

where T_0 is the environmental temperature, $\dot{Q}_j$ is the time rate of heat transfer at the location on the boundary, T_j is the boundary temperature, $\dot{W}_{cv}$ is the work produced in the control volume, $\dot{m}$ is the mass flow rate, ψ is the specific flow exergy, and $\dot{E}x_d$ is the rate of exergy destruction in the control volume while the subscripts *in* and *out* denote inlet and outlet, respectively. The specific flow exergy of the refrigerant can be obtained from

$$\psi = (h - h_0) - T_0(s - s_0) \tag{5}$$

where subscript "0" denotes the dead state.

Assuming that the compressor operates adiabatically, the compressor exergy destruction rate can be evaluated from

$$\dot{E}x_{d,comp} = \dot{m}_r(\psi_1 - \psi_2) + \dot{W}_{comp} \tag{6}$$

The outdoor unit exergy destruction rate can be determined from

$$\dot{E}x_{d,ou} = \dot{m}_r(\psi_7 - \psi_8) + \dot{m}_{a,ou}(\psi_{a,E} - \psi_{a,F}) \tag{7}$$

where $\dot{m}_{a,ou}$ indicates the air mass flow rate blown across the outdoor unit. The specific flow exergies of air at locations E and F can be obtained from [35]

$$\psi_a = (c_{p,a} + \omega c_{p,v})T_0\left[\left(\frac{T}{T_0}\right) - 1 - \ln\left(\frac{T}{T_0}\right)\right] + \left[(1 + 1.6078\omega)R_aT_0\ln\left(\frac{P}{P_0}\right)\right] + R_aT_0\left\{(1 + 1.6078\omega)\ln\left(\frac{1 + 1.6078\omega_0}{1 + 1.6078\omega}\right) + 1.6078\omega\ln\left(\frac{\omega}{\omega_0}\right)\right\} \tag{8}$$

where $c_{p,a}$ and $c_{p,v}$ are specific heats of air and water vapour, respectively, R_a is the ideal gas constant of dry air, ω is the specific humidity and P is the pressure.

Assuming that the expansion valve operates adiabatically, the exergy destruction rate in the TXV can be found from

$$\dot{E}x_{d,TXV} = \dot{m}_r(\psi_6 - \psi_7) \tag{9}$$

The indoor unit exergy destruction rate can be evaluated from

$$\dot{E}x_{d,iu} = \dot{m}_r(\psi_3 - \psi_4) + \dot{m}_{a,iu}(\psi_{a,B} - \psi_{a,C}) \tag{10}$$

The specific flow exergies of air at locations B and C can be obtained from Eq. (8).

The exergy destruction in the reversing valve can be ignored because this component has been insulated very well, and the heat transfer rate between the two refrigerant streams passing through it is very low. Then, the total exergy destruction rate in the AHP can be evaluated from the summation of the individual destruction rates, i.e.

$$\dot{E}x_{d,tot} = \dot{E}x_{d,comp} + \dot{E}x_{d,ou} + \dot{E}x_{d,TXV} + \dot{E}x_{d,iu} \tag{11}$$

Uncertainty analysis

The uncertainties of the performance parameters of the AHP system were determined using the method proposed by Moffat [36]. In this method, if a function y is to be calculated from a set of totally n measured variables, namely $x_1, x_2, \ldots, x_n$, the uncertainty of the y function can be determined from

$$u_y = \sqrt{\sum_{i=1}^{n}\left(\frac{\partial y}{\partial x_i}u_{x_i}\right)^2} \tag{12}$$

where u_{x_i} indicates the uncertainty of the measured variable.

Considering that the y function is the performance parameters defined by Eqs. (1−3), (6), (7) and (9−11) and using the test results along with the uncertainties of the instruments specified in Table 2, the absolute uncertainties of the performance parameters can be calculated from Eq. (12). With the aid of Engineering Equation Solver software [37], the uncertainty bands of the performance parameters of the AHP system have been evaluated and the results are presented in Table 4 for both refrigerants.

Table 4 Absolute uncertainties of the performance parameters of the AHP system

Parameter	R134a	R1234yf
$\dot{Q}_{iu}$/kW	±0.011–0.017	±0.012–0.019
$\dot{W}_{comp}$/kW	±0.010–0.015	±0.012–0.017
COP	±0.029–0.104	±0.033–0.123
$\dot{E}x_{d,comp}$/kW	±0.043–0.083	±0.046–0.088
$\dot{E}x_{d,ou}$/kW	±0.036–0.074	±0.038–0.079
$\dot{E}x_{d,TXV}$/kW	±0.006–0.011	±0.008–0.014
$\dot{E}x_{d,iu}$/kW	±0.006–0.007	±0.006–0.007
$\dot{E}x_{d,tot}$/kW	±0.011–0.015	±0.012–0.016

Total equivalent warming impact (TEWI) of the experimental AHP system

The AAC and AHP systems can cause warming impact on the environment directly or indirectly. Their direct impact is due to the refrigerant emissions caused by leakage, partial recovery of the refrigerant and disposal of the system. Their indirect impact, on the other hand, is due to the CO_2 emissions caused by the burning of the fuel to generate the mechanical power required for driving the AAC and AHP systems. The sum of these two impacts is represented by the total equivalent warming impact (TEWI), which can be calculated from the equation below in kg CO_2 equivalent [22, 38]

$$\mathrm{TEWI} = \mathrm{GWP}\ L\ N\ m_r + \mathrm{GWP}\ m_r(1-\alpha) + \left(\mathrm{FC_{pow}}\frac{D_{ann}}{10000} + \mathrm{FC_m}\frac{m_{AHP}}{100}\frac{D_{ann}}{10000}\right)\frac{\mathrm{COP_{R134a}}}{\mathrm{COP_r}}\beta N \quad (13)$$

where L is the annual refrigerant leakage ratio and m_r is the refrigerant charge in the system, respectively, while N is the lifetime of the system and α is the refrigerant recovery factor. Moreover, FC_{pow} indicates the volumetric fuel consumption per 10,000 km driving to power the AHP using R134a, D_{ann} shows the annual driving distance in km, FC_m denotes the volumetric fuel consumption for incremental mass changes of the vehicle per 100 kg mass of the AHP system per 10,000 km driving and m_{AHP} means the mass of the AHP system. Finally, β is the CO_2 emission factor of the fuel used in the vehicle in kg CO_2 per unit fuel volume, COP_{R134a} is the COP of the system using R134a while COP_r is the COP of the system using the tested refrigerant, i.e. COP_{R134a} or $COP_{R1234yf}$. The sum of the first and second terms in Eq. (13) accounts for the direct impact while the third term gives the indirect impact of the system on global warming.

The TEWI of the experimental AHP system was evaluated using the assumptions or experimental values described below:

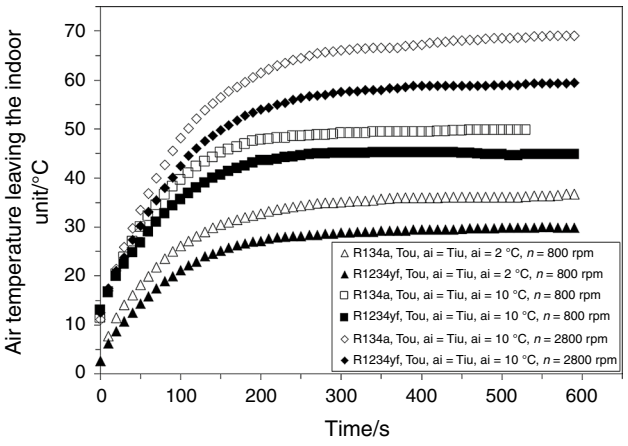

Fig. 3 Conditioned air temperature as a function of time

- The GWP of R134a is 1430. Although the GWP of R1234yf is reported as lower than 1 [6], it is assumed as 1.
- The annual leakage ratio is 0.2 (i.e. 20%) [22], and the lifetime of the system is 15 years [22].
- The refrigerant charges used in the experimental system are 1.85 kg and 1.65 kg for R134a and R1234yf, respectively.
- The recovery factor is 0.75 [39].
- The volumetric fuel consumption to power the AHP with R134a is 60 L of gasoline per 10,000 km driving.
- The volumetric fuel consumption due to the increase in the vehicle mass is 57 L of gasoline per 100 kg mass of the AHP system per 10,000 km driving [38].
- The mass of the AHP system is 15 kg [22], and the annual driving distance is 12,000 km.
- The CO_2 emission factor of the fuel is 2.31 kg CO_2 per L gasoline.
- The COP_{R134a} and $COP_{R1234yf}$ are assumed to be equal to the mean experimental COP values, namely 3.5644 and 3.4061, respectively.

The results of TEWI calculations are presented in the next section.

Results and discussion

Various performance merits of the experimental AHP using R1234yf are presented in Figs. 3–11 relative to the baseline system using R134a.

The variation in the conditioned air temperature leaving the indoor unit of the AHP with respect to time is reported in Fig. 3. It usually took about 5–7 min to the reach steady state for both refrigerant cases depending on the compressor speed and air inlet temperatures. In the most critical

test performed at the compressor speed of 800 r min^{-1} and air inlet temperature of 2 °C, the R134a and R1234yf systems yielded the steady-state conditioned air temperatures of 36.5 °C and 29.9 °C, respectively. On the other hand, when the air inlet temperature was 10 °C for 800 r min^{-1}, the R134a and R1234yf systems resulted in the steady-state conditioned air temperatures of about 49.4 °C and 44.8 °C, respectively. Furthermore, when the compressor speed was increased to 2800 r min^{-1} for 10 °C air inlet temperature, the R134a and R1234yf systems provided the steady-state conditioned air temperatures of about 68.7 °C and 59.2 °C, respectively. Because the latent heat of vaporization of R134a is 21–28% higher than that of R1234yf depending on the saturation temperature, R134a absorbs more heat from the ambient air in outdoor unit, thus rejecting more heat in the indoor unit and providing higher conditioned air temperature.

The steady-state conditioned air temperature leaving the indoor unit of the AHP with respect to the compressor speed is shown in Fig. 4. The higher the compressor speed, the higher the conditioned air temperature for both refrigerants. Furthermore, the conditioned air temperature gets higher when the air temperatures entering the outdoor and indoor units increase simultaneously. For 2 °C air inlet temperature, the AHP with R1234yf resulted in 4.2–6.6 °C lower conditioned air temperature compared to the system with R134a in the compressor speed range of 800–1600 r min^{-1}. On the other hand, for 10 °C air inlet temperature, the AHP system with R1234yf yielded 3.3–10.8 °C lower conditioned air temperature in the compressor speed range of 800–2800 r min^{-1}.

The refrigerant mass flow rate in the AHP with respect to the compressor speed is indicated in Fig. 5. The mass flow rate gets higher with rising compressor speed and air temperatures entering the outdoor and indoor units for both refrigerants. When the air temperature entering the outdoor unit increases, so does the refrigerant mass flow rate. However, it decreases on increasing the air temperature entering the indoor unit. When both air temperatures increase simultaneously, the effect of the former one overweighs that of the latter, thus promoting the refrigerant mass flow rate. Because the vapour density of R1234yf is higher than that of R134a for the same saturation temperature, it yields higher refrigerant mass flow rate. For the air inlet temperatures of 2 °C and 10 °C, the mass flow rate of R1234yf was higher than that of R134a in the ranges of 9.7–13.9% and 4.4–8.9%, respectively.

The heating capacity of the AHP with respect to the compressor speed is reported in Fig. 6. Since the refrigerant mass flow rate increases with the compressor speed, so does the heating capacity for both refrigerants. Furthermore, when the air temperature incoming the outdoor unit increases, more heat is transferred from the air stream to

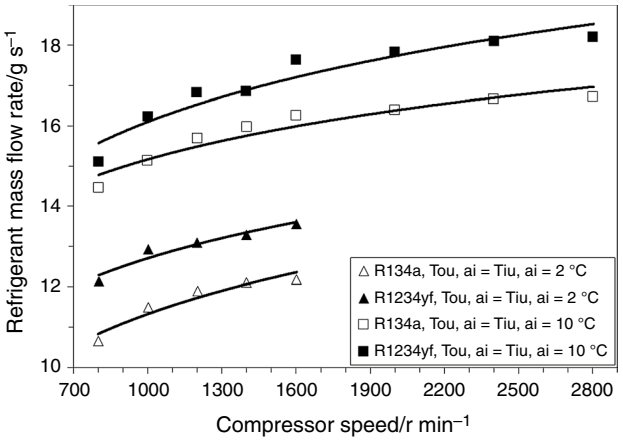

Fig. 5 Refrigerant mass flow rate as a function of the compressor speed

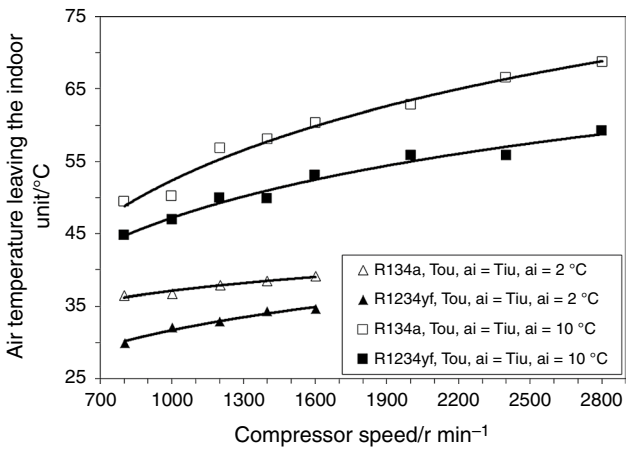

Fig. 4 Conditioned air temperature as a function of the compressor speed

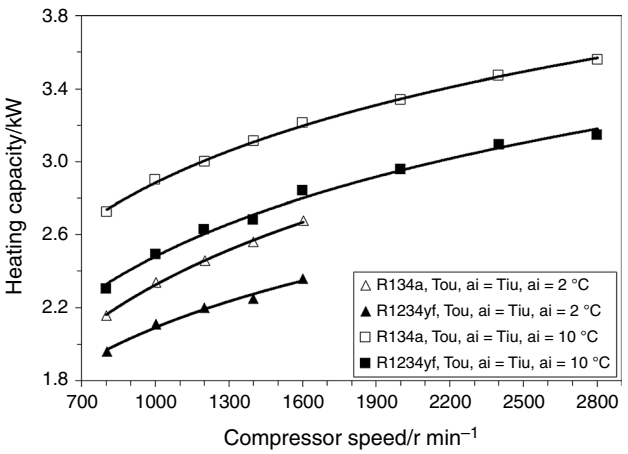

Fig. 6 Heating capacity as a function of the compressor speed

the evaporating refrigerant in this unit. Consequently, the amount of heat transferred to the conditioned air stream in the indoor unit increases, thus causing a higher heating capacity. The AHP system using R134a and R1234yf provided heating capacities in the ranges of 2.15–3.47 kW and 1.96–3.14 kW, respectively. For the air inlet temperature of 2 °C, the AHP with R1234yf yielded 9.2–12.2% lower heating capacity than the system with R134a. For the air inlet temperature of 10 °C, on the other hand, the system with R1234yf yielded 10.9–15.4% lower heating capacity. As a result of the higher latent heat of vaporization of R134a, the system with R134a provides a higher heating capacity despite its lower refrigerant mass flow rate. Although both refrigerants offer considerable heating capacities, they are unsatisfactory to meet the comfort heating requirement of the passenger cabin in an automobile.

The compressor power of the AHP with respect to the compressor speed is shown in Fig. 7. The compressor power gets higher with rising compressor speed and air temperatures entering the outdoor and indoor units. Because rising the compressor speed promotes the refrigerant mass flow rate and pressure ratio across the compressor, the compressor power gets higher. Furthermore, rising the air temperatures increase the compressor pressure ratio, thereby causing higher compressor power. Although R1234yf operates with higher refrigerant mass flow rates, it experiences lower compressor pressure ratios relative to R134a. It is seen that the effect of the latter overweighs that of the former one. The AHP system using R134a and R1234yf absorbed compressor powers in the ranges of 0.46–1.40 kW and 0.43–1.29 kW, respectively. The AHP system with R1234yf absorbed 5.4–9.2% and 5.5–10.4% less compressor power in comparison with the system with R134a for the air inlet temperatures of 2 °C and 10 °C, respectively.

The COP for heating of the AHP with respect to the compressor speed is presented in Fig. 8. The COP

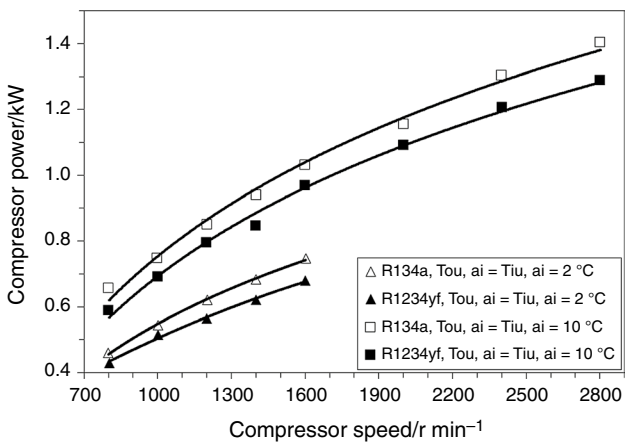

Fig. 7 Compressor power as a function of the compressor speed

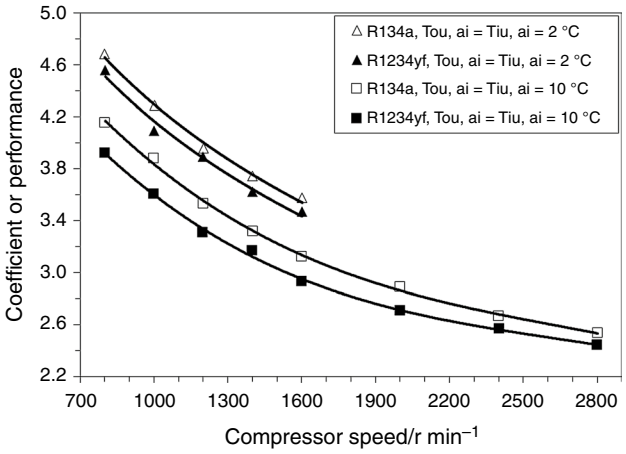

Fig. 8 Coefficient of performance as a function of the compressor speed

decreases with rising either the compressor speed or air temperatures entering the outdoor and indoor units for both refrigerant cases. A rise in the compressor speed leads to a moderate increase in the heating capacity but a more abrupt increase in the compressor power. Consequently, the COP for heating drops with rising compressor speed. Similarly, when the air inlet temperatures increase, the compressor power gets higher more abruptly than the heating capacity does, thus reducing the COP. The AHP system using R134a and R1234yf resulted in COP values in the ranges of 2.54–4.68 and 2.44–4.56, respectively. Although R1234yf absorbs slightly less compressor power, it provides considerably lower heating capacities, thus resulting in lower COP values relative to R134a. For the air inlet temperatures of 2 °C and 10 °C, the AHP with R1234yf yielded 1.6–4.5% and 3.7–7.1% lower COP compared to the system with R134a, respectively.

The compressor discharge temperature of the AHP with respect to the compressor speed is reported in Fig. 9. The higher the compressor speed or air inlet temperatures, the higher the compressor discharge temperature for both refrigerant cases. Rising either the compressor speed or air inlet temperatures promote the pressure ratio across the compressor and refrigerant mass flow rate, thus leading to elevated compressor discharge temperature. High discharge temperature deteriorates the compressor lubrication oil, thus decreasing the lifetime of the compressor. However, it promotes the heat rejection in the indoor unit, thus increasing the heating capacity. For the air inlet temperatures of 2 °C and 10 °C, the R1234yf system yielded 13.8–20.8 °C and 13.9–21.6 °C lower discharge temperature relative to the R134a system, respectively. Lower discharge temperature provided by the AHP system with R1234yf is one of the reasons of its poorer heating capacity reported in Fig. 6.

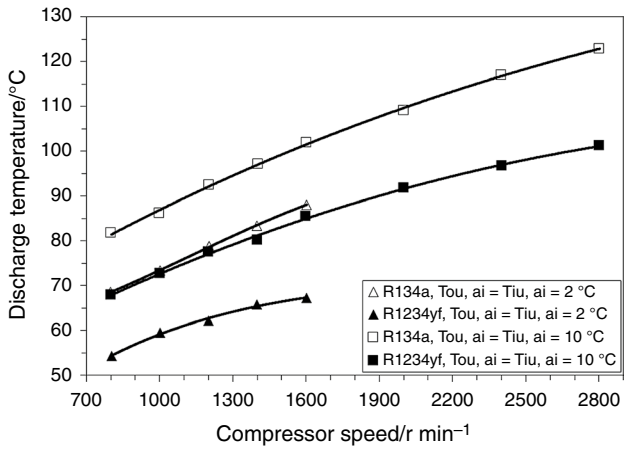

Fig. 9 Compressor discharge temperature as a function of the compressor speed

The exergy destruction rates in the AHP components are shown in Fig. 10 for two different air temperatures incoming the outdoor and indoor units at 1000 r min^{-1} compressor speed. The outdoor unit destructed the largest exergy, followed by the indoor unit, expansion device and compressor in decreasing order for both refrigerant cases. The exergy destructions in the outdoor and indoor units are due to the heat transfer between the refrigerant and air streams. The exergy destruction rates in these units increase with rising temperature difference between these two streams. In the outdoor unit, the R1234yf system destructed 5.6–19.2% more exergy than the R134a one. Because R1234yf yields a lower compressor discharge temperature, it causes a lower average temperature difference between the refrigerant and air streams in the indoor unit, thus causing less exergy destruction in the indoor unit compared to R134a. The AHP with R1234yf yielded 25.5–39.8% less indoor unit exergy destruction rates than that with R134a. Despite lower compressor pressure ratios experienced with R1234yf, due to higher refrigerant flow rates, the compressor and expansion device of the R1234yf system destruct larger exergy relative to the system with R134a. Moreover, both the refrigerant mass flow rate and compressor pressure ratio increase with rising air inlet temperatures, thus destructing more exergy in the compressor and expansion device. Consequently, in comparison with the R134a system, the R1234yf system destructed 7.9–14.1% and 25.8–26.9% more exergy in the compressor and TXV, respectively, as a function of the air inlet temperatures.

The total exergy destruction rate per unit heating capacity of the AHP with respect to the compressor speed is reported in Fig. 11. Because the exergy destruction rate in each component of the AHP increases more abruptly than the heating capacity does with rising either the compressor speed or air inlet temperatures, the total exergy destruction rate per unit heating capacity increases with them as well. The pressure ratio across the compressor increases on rising the compressor speed, thereby decreasing the evaporating temperature and increasing the condensing temperature. As a result, the temperature difference between the air and refrigerant streams increases, and the exergy destruction rates in the evaporator and condenser get higher. Moreover, rising pressure ratio leads to larger exergy destructions in the compressor and TXV. The total exergy destruction rate per unit heating capacity of the R1234yf system was 3.1–19.2% and 8.6–16.1% higher than that of the R134a system for the air inlet temperatures of 2 °C and 10 °C, respectively. These results agree with the lower COP values offered by the R1234yf system as shown in Fig. 8.

Based on the assumptions and experimental values described in the previous section, the TEWI of the experimental AHP system with R134a and R1234yf is reported in Table 5. It is seen that the impact of the direct refrigerant emissions from the R134a system is substantially greater than that from the R1234yf system. However, the R1234yf

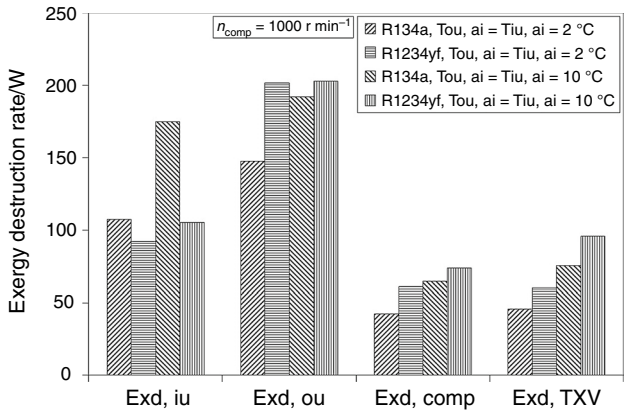

Fig. 10 Exergy destruction rates in the components

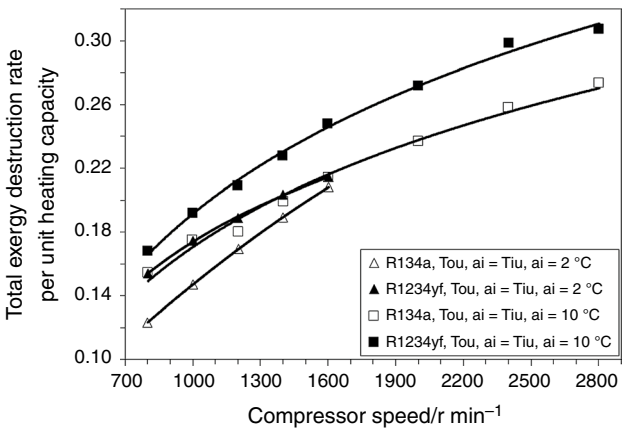

Fig. 11 Total exergy destruction rate per unit heating capacity as a function of the compressor speed

Table 5 TEWI of the AHP system using R134a and R1234yf

Impact	R134a	R1234yf
Direct impact/kg equivalent CO_2	8598	5
Indirect impact/kg equivalent CO_2	2850	2983
TEWI//kg equivalent CO_2	11,448	2988

system yields a slightly higher impact due to the powering of the system. Consequently, the use of R1234yf in the AHP causes a considerably lower TEWI relative to the use of R134a. These TEWI results agree with those reported by Hamza and Khan [39] and Tuchowski and Kurts-Orecka [40].

In accordance with the findings of this study, insufficient heating capacities for R134a AHP systems were also reported by Hosoz and Direk [12] and Lee and Lee [16]. Furthermore, Direk and Yuksel [30] also found that their R1234yf AHP performed poorly in terms of the heating capacity and COP compared with the R134a system.

Conclusions

An experimental AHP was developed by adding a reversing valve, another expansion valve and hand valves to the components of an AAC system belonging to a compact automobile. The performance merits of the AHP were evaluated for R134a and R1234yf by changing the compressor speed in the range of 800–2800 r min^{-1} for two different temperatures of the air streams incoming the outdoor and indoor units, namely 2 °C and 10 °C. The following conclusions can be extracted from the comparison of the experimental results:

- The AHP with R1234yf resulted in steady-state conditioned air temperatures ranging between 29.9 and 59.3 °C, which were 3.3–10.8 °C lower than those provided by the system with R134a.
- The AHP with R1234yf yielded 4.4–13.9% higher refrigerant mass flow rates in comparison with the system with R134a.
- The AHP with R1234yf yielded heating capacities ranging between 1.96 and 3.14 kW, which were 9.2–15.4% lower in comparison with the system with R134a.
- The AHP with R1234yf resulted in COP values ranging between 2.44 and 4.56 kW. Although it absorbed 5.4–10.4% less compressor power, it yielded 1.6–7.1% lower COP relative to the R134a system.
- The AHP with R1234yf provided 13.8–21.6 °C lower compressor discharge temperatures compared to the system with R134a.
- For both refrigerant cases, the component causing the largest exergy destruction was the outdoor unit, followed by the indoor unit, TXV and compressor in reducing order.
- The AHP with R1234yf caused 3.1–19.2% higher total exergy destruction rate per unit heating capacity in comparison with the R134a system.
- The TEWI of the AHP with R134a is 11,448 kg equivalent CO_2, while that with R1234yf is only 2988 kg equivalent CO_2.

These findings reveal that R1234yf can be used in AHP systems in expense of lower heating capacity and COP relative to R134a. The heating capacity of the system for both refrigerants is too low to meet the comfort heating requirement of the passenger cabin in an automobile. Therefore, it can presently be used to provide supplemental heating. However, the performance of AHP systems can be improved by increasing the size of the outdoor unit or its air flow rate to promote the heat absorbed from the ambient air. Furthermore, employing a compressor with larger stroke volume and compression ratio will increase both the refrigerant flow rate and compressor discharge temperature, thus promoting the heating capacity. Moreover, the performance of the AHP systems with R1234yf can be increased by using an internal heat exchanger between the suction and discharge lines of the refrigeration circuit to drop the enthalpy of the refrigerant entering the outdoor unit. In this case, the refrigerant can absorb more heat from the ambient air in the outdoor unit, thus dissipating more heat in the indoor unit, which leads to higher heating capacity and COP.

References

1. UNEP. Montreal Protocol on substances that deplete the ozone layer, final act. United Nations Environment Programme. 1987. https://www.unenvironment.org/resources/report/montreal-protocol-substances-deplete-ozone-layer-final-act. Accessed 5 Jan 2020.
2. Lee Y, Jung D. A brief performance comparison of R1234yf and R134a in a bench tester for automobile applications. Appl Therm Eng. 2012;35:240–2.
3. EU. Regulation (EU) No 517/2014 of the European Parliament and of the Council of 16 April 2014 on fluorinated greenhouse gases and repealing Regulation (EC) No 842/2006. Official J European Union. 2014; L 150/195.
4. Zhang Z, Wang J, Feng X, Chang L, Chen Y, Wang X. The solutions to electric vehicle air conditioning systems: a review. Renew Sust Energ Rev. 2018;91:443–63.
5. Ma Y, Liu Z, Tian H. A review of transcritical carbon dioxide heat pump and refrigeration cycles. Energy. 2013;55:156–72.
6. Hodnebrog Ø, Etminan M, Fuglestvedt JS, Marston G, Myhre G, Nielsen CJ, Shine KP, Wallington TJ. Global warming potentials and radiative efficiencies of halocarbons and related compounds: a comprehensive review. Rev Geophys. 2013;51:300–78.
7. Wang CC. System performance of R-1234yf refrigerant in air-conditioning and heat pump system-an overview of current status. Appl Therm Eng. 2014;73:1412–20.

8. Peng Q, Du Q. Progress in heat pump air conditioning systems for electric vehicles: a review. Energies. 2016;9:240. https://doi.org/10.3390/en9040240.
9. Tamura T, Yakumaru Y, Nishiwaki F. Experimental study on automotive cooling and heating air conditioning system using CO2 as a refrigerant. Int J Refrig. 2005;28:1302–7.
10. Wang D, Yu B, Hu J, Chen L, Shi J, Chen J. Heating performance characteristics of CO_2 heat pump system for electrical vehicle in a cold climate. Int J Refrig. 2018;85:27–41.
11. Wang D, Yu B, Li W, Shi J, Chen J. Heating performance evaluation of a CO_2 heat pump system for an electrical vehicle at cold ambient temperatures. Appl Therm Eng. 2018;142:656–64.
12. Hosoz M, Direk M. Performance evaluation of an integrated automotive air conditioning and heat pump system. Energ Convers Manage. 2006;47:545–59.
13. Lee DY, Cho CW, Won JP, Park YC, Lee MY. Performance characteristics of mobile heat pump for a large passenger electric vehicle. Appl Therm Eng. 2013;50:660–9.
14. Hosoz M, Direk M, Yigit KS, Canakci M, Turkcan A, Alptekin E, Sanli A. Performance evaluation of an R134a automotive heat pump system for various heat sources in comparison with baseline heating system. Appl Therm Eng. 2015;78:419–27.
15. Wang Z, Wei M, Peng F, Liu H, Guo C, Tian G. Experimental evaluation of an integrated electric vehicle AC/HP system operating with R134a and R407C. Appl Therm Eng. 2016;100:1179–88.
16. Lee HS, Lee MY. Steady state and start-up performance characteristics of air source heat pump for cabin heating in an electric passenger vehicle. Int J Refrig. 2016;69:232–42.
17. Zilio C, Brown JS, Schiochet G, Cavallini A. The refrigerant R1234yf in air conditioning systems. Energy. 2011;36:6110–20.
18. Mota-Babiloni A, Navarro-Esbri J, Barragan-Cervera A, Moles F, Peris B. Drop-in energy performance evaluation of R1234yf and R1234ze(E) in a vapour compression system as R134a replacements. Appl Therm Eng. 2014;71:259–65.
19. Cho H, Park C. Experimental investigation of performance and exergy analysis of automotive air conditioning systems using refrigerant R1234yf at various compressor speeds. Appl Therm Eng. 2016;101:30–7.
20. Prabakaran R, Lal DM, Devotta S. Effect of thermostatic expansion valve tuning on the performance enhancement and environmental impact of a mobile air conditioning system. J Therm Anal Calorim. 2020. https://doi.org/10.1007/s10973-019-09224-2.
21. Huang L. Energy and exergy performance comparison of different HFC/R1234yf mixtures in vapor-compression cycles. J Therm Anal Calorim. 2020;140:2447–59.
22. Abraham JDAP, Mohanraj M. Thermodynamic performance of automobile air conditioners working with R430A as a drop-in substitute to R134a. J Therm Anal Calorim. 2019;136:2071–86.
23. Gill J, Singh J, Ohunakin OS, Adelekan DS. ANN approach for irreversibility analysis of vapor compression refrigeration system using R134a/LPG blend as a replacement of R134a. J Therm Anal Calorim. 2019;135:2495.
24. Gill J, Singh J, Ohunakin OS, Adelekan DS. Exergy analysis of vapor compression refrigeration system using R450a as replacement of R134a. J Therm Anal Calorim. 2019;136:857–72.
25. Zou H, Huang G, Shao S, Zhang X, Tian C, Zhang X. Experimental study on heating performance of an R1234yf heat pump system for electric cars. Energy Procedia. 2017;142:1015–21.
26. Direk M, Yuksel F. Comparative experimental evaluation on heating performance of a mobile air conditioning system using R134a, R1234ze(E), R152a and R444a. J Therm Sci Technol. 2019;39:31–8.
27. Wang Z, Wei M, Guo C, Zhao M. Enhance the heating performance of an electric vehicle AC/HP system under low temperature. Energy Procedia. 2017;105:2384–9.
28. Zhang K, Li M, Yang C, Shao Z, Wang L. Exergy analysis of electric vehicle heat pump air conditioning system with battery thermal management system. J Therm Sci. 2020;29:408–22.
29. Ozcan HG, Hepbasli A, Gunerhan H. Performance evaluation of a mobile air conditioning unit: an exergetic approach. Int J Exergy. 2019;28:183.
30. Direk M, Yuksel F. Experimental evaluation of an automotive heat pump system with R1234yf as an alternative to R134a. Arab J Sci Eng. 2020;45:719–28.
31. Devecioglu AG, Oruc V. A comparative energetic analysis for some low-GWP refrigerants as R134a replacements in various vapor compression refrigeration systems. J Therm Sci Technol. 2018;38:51–61.
32. Arora P, Seshadri G, Tyagi AK. Fourth-generation refrigerant: HFO 1234yf. Curr Sci. 2018;115:1497.
33. Lemmon EW, Huber ML, McLinden MO. Reference Fluid Thermodynamic and Transport Properties (REFPROP), Version 9.1, in NIST Standard Reference Database 23. Gaithersburg: National Institute of Standards and Technology; 2013.
34. Cho H, Lee H, Park C. Performance characteristics of an automobile air conditioning system with internal heat exchanger using refrigerant R1234yf. Appl Therm Eng. 2013;61:563–9.
35. Ozgener O, Hepbasli A. Modeling and performance evaluation of ground source (geothermal) heat pump systems. Energy Build. 2007;39:66–75.
36. Moffat RJ. Describing the uncertainties in the experimental results. Exp Therm Fluid Sci. 1988;1:3–17.
37. Klein SA. EES: Engineering Equation Solver, Version 10.167. F-Chart Software; 2016.
38. Fischer SK. Total equivalent warming impact: a measure of the global warming impact of CFC alternatives in refrigeration equipment. Int J Refrig. 1993;16:423–8.
39. Hamza A, Khan TA. Comparative performance of low-GWP refrigerants as substitutes for R134a in a vapor compression refrigeration system. Arab J Sci Eng. 2020. https://doi.org/10.1007/s13369-020-04525-3.
40. Tuchowski W, Kurtz-Orecka K. The influence of refrigerants used in air-conditioning systems in motor vehicles on the environment. In: Ball P, Huatuco LH, Howlett RJ, Setchi R, editors. Smart innovation, systems and technologies–proceedings of the 6th international conference on sustainable design and manufacturing. Singapore: Springer Nature; 2019. pp. 605–14.